

Algebraic Iterative Reconstruction-Reprojection (AIRR) Method for High Performance Sparse-View CT Reconstruction

Ali Pour Yazdanpanah^{1,*}, Emma E. Regentova¹ and George Bebis²

¹ Department of Electrical and Computer Engineering, University of Nevada, Las Vegas, NV 89154, USA

² Department of Computer Science and Engineering, University of Nevada, Reno, NV 89557, USA

Received: 11 Mar. 2016, Revised: 7 Jul. 2016, Accepted: 9 Jul. 2016

Published online: 1 Nov. 2016

Abstract: The reconstruction from sparse- or few-view projections is one of important problems in computed tomography limited by the availability or feasibility of a large number of projections. Working with a small number of projections provides a lower radiation dose and a fast scan time, however an error associated with the sparse-view reconstruction increases significantly as the space sparsity increases that may cause the reconstruction process to diverge. The iterative reconstruction-re-projection (IRR) algorithm which uses filtered back projection (FBP) reconstruction has been used for the sparse-view computed tomography applications for several years. The IRR-TV method has been developed as a higher performance alternative to the IRR method by adding the total variation (TV) minimization. Here, we propose an algebraic iterative reconstruction-re-projection (AIRR) algorithm with the shearlet regularization. The AIRR coupled with the shearlet regularization in image space attains a better estimation in the projection space and yielded a higher performance based on subjective and objective quality metrics.

Keywords: Iterative Reconstruction-Reprojection, Sparse-View CT Reconstruction, Algebraic Computed Tomography.

1 Introduction

Computed Tomography (CT) is used for medical diagnostics, non-destructive testing, airport baggage screening and also considered for cargo inspection for determining treats, such as explosives and Special Nuclear Materials (SNM) [1,2,3,4]. For medical, security or industrial applications of CT a limited number of views is an option for whether reducing the radiation dose or screening time, and the cost in either case. In the applications such as non-destructive testing and inspection of large objects, the scanning of objects can take up to minutes for only one projection. When the neutron source is used rather than the photon, the scanning will take on a long time even for small objects, such as passenger luggage, because of the large number of neutrons required for producing the quality images for the analyses.

There are also various practical reasons behind the insufficient data acquisition. Such constraints are due to the imaging component, geometry modeling, or ionizing radiation exposure. Gaps present in the projection data

caused by a bad detector bins is another reason causing the limited number of angles. Thus, a reasonably low number of angular views will be made available for the reconstruction algorithm which is expected to produce images whose quality is suitable for the analyses they are acquired for.

The reconstruction under the sparse-view always causes artifacts which are more noticeable when the filtered back-projection method is used. The traditional IRR algorithm [5,6] strives to extrapolate missing projections by going back and forth between projections and the image domain. Candes et al. [7], proposed the FT-TV method that reconstructs the sparse gradient images accurately from the Fourier transform (FT) samples by using minimization. The IRR-TV reconstruction method [8] separates the reconstruction process in the image and the projection domains and applies the total variation (TV) in image domain to obtain the sparse-view projections. Although the IRR-TV method has a higher performance compared to the traditional IRR method, the number of iterations is

* Corresponding author e-mail: pouryazd@unlv.nevada.edu

strictly controlled for avoiding the divergence point which takes place very soon, i.e., after just few iterations.

In this paper, we propose an algebraic iterative reconstruction-reprojection (AIRR) algorithm with the shearlet regularization. Shearlets have already proved its potential for image denoising [9, 10] and they are efficient in representing edges of various orientations, strength and scales, that is those that constitute the object shape and describe textures, and thus the inclusion of their regularization promises a better performance for the above problem.

The paper is organized as follows. In Section 2, the background information is provided. The proposed algebraic iterative reconstruction-reprojection method is presented in Section 3. In Section 4, we demonstrate results; Conclusions are drawn in Section 5.

2 Methods

Here, we review the iterative reconstruction-reprojection (IRR) method. The IRR method works as a reconstruction method that in order to estimate the missing angular projection it alternate backprojection and reprojection spaces and it is mathematically equivalent to the Gerchberg-Papoulis algorithm that iterates in the Fourier domain and converges for band-limiting signals [11, 12]. The IRR method includes three steps:

$$g^i(r, \theta) = h(r) * p^i(r, \theta), \quad (1)$$

$$f^i(r, \theta) = \int_0^{2\pi} g^i(x \cos(\theta) + y \sin(\theta)) d\theta, \quad (2)$$

$$p_{rep}^{i+1}(r, \theta) = \int_{-L}^L f^i(r \cos(\theta) - t \sin(\theta), r \sin(\theta) + t \cos(\theta)) dt. \quad (3)$$

In the above equations, $g^i(r, \theta)$ is the filtered projection data for reconstruction in the i_{th} step and $h(r)$ is the filter in FBP process in the time-domain. $p_{rep}^i(r, \theta)$ is the reprojection data computed from f^{i-1} which is the $(i-1)_{th}$ reconstructed image. The error propagation introduced in the backprojection and reprojection iterations is the main disadvantage of the IRR method. [5], authors combined equation (2) and equation (3) into one step in projection space to reduce the interpolation error as follows:

$$p_{rep}^{i+1}(r, \theta) = 2L \sin(\theta_m) g^i(r, \theta) + \int_0^\pi \int_{L \cos(\theta - \hat{\theta} + \theta_m)}^{L \cos(\theta - \hat{\theta} - \theta_m)} \frac{g^i(\hat{r}, \hat{\theta})}{\sin(\theta - \hat{\theta})} d\hat{r} d\hat{\theta}. \quad (4)$$

where $\theta_m = \cos^{-1}(l/L)$ and L is the radius of the reconstructed region. This method is computationally intense, and the divergence is observed after few iterations.

Xinhui Duan et. al. in [8] used the total variation (TV) minimization to improve the IRR accuracy by adding the TV minimization layer to the framework. The TV-based model is described as below:

$$\min TV(f) \quad st. \quad Mf = p, \quad (5)$$

where p is the sparse sparse-view projection data, and M is a measurement matrix.

$$TV(f) = \sqrt{(f_{x,y} - f_{x-1,y})^2 + (f_{x,y} - f_{x,y-1})^2}, \quad (6)$$

where $TV(f)$ is the total variation of the 2D image, f . The complete process is described then by equation (7).

$$\hat{f} = \hat{f} - d \frac{\partial TV(\hat{f})}{\partial \hat{f}}. \quad (7)$$

Where \hat{f} is the reconstructed image from projection p using filtered back projection method. The IRR+TV method performs much better than its traditional counterpart, under the strictly controlled number of iterations.

3 AIRR

In the proposed AIRR method the reconstruction is formulated as a linear problem for two different models: a noise-free model described by equation (8) and the noisy model given by equation (9).

$$Af = b. \quad (8)$$

$$Af + n = b. \quad (9)$$

Where $b \in R^N$ is the projection data, $f \in R^M$ is the reconstruction result, and $A \in R^{N \times M}$ is the system geometry matrix. The AIRR algorithm includes three processes in each iteration:

1. Iterative Algebraic Reconstruction.
2. Shearlet-based denoising.
3. Reprojection

3.1 Iterative Algebraic Reconstruction

Instead of traditional FBP method, we use simultaneous algebraic reconstruction technique (SART) [13, 15] by introducing a stopping criteria. The convergence of the SART algorithm was proved in [13, 15].

The reconstruction of f is performed by iterating according to the following:

$$f^{k+1} = f^k + \lambda_k C^{-1} V A^T W (b - A f^k) \quad (10)$$

where $V = \text{diag}(1/\sum_{i=1}^N a_{i,j})$, for $j = 1, \dots, M$ and $W = \text{diag}(1/\sum_{j=1}^M a_{i,j})$ for $i = 1, \dots, N$. Also C is the exponential weighting matrix used to moderate the errors corresponding to the large values of b [14, 16].

$$C = \text{diag}(c_0, c_1, \dots, c_i) \quad \text{when} \quad c_i = e^{-E[b_i]} \quad (11)$$

We use the projection values as an estimate for $E[b_i]$. Algebraic reconstruction is performed with the non-negativity constraint, $\hat{f}(x, y) = 0$ for $f(x, y) < 0$, when $\hat{f} = f^q$ if the iteration stops at $k = q$.

The discrepancy principle criteria is used for the stopping condition by finding the smallest k such that

$$\|W^{1/2}(b - A f^k)\|_2 \leq \tau \delta \quad (12)$$

where τ can be found experimentally.

3.2 Discrete Shearlet-Based Denoising

The discrete shearlet transformation (DST) was presented in [17, 18, 19, 20]. Let $\psi_{a,s,t}(x)$ denote the shearlet basis functions or simply shearlets. The continuous shearlet transformation (CST) of image $f(x)$ is defined in

$$SH_\varphi(a, s, t) = \int_{R^2} f(x) \psi_{a,s,t}(t-x) dx \quad (13)$$

where $s \in R$, $a \in R$, and $t \in R^2$ define the orientation, scale, and location in the spatial domain, respectively and $\hat{f}(x) \in R^2$ is a two dimensional reconstructed image.

Shearlets are shaped by dilating, shearing and translating the mother shearlet $\psi_{a,s,t} \in R^2$, as below:

$$\psi_{a,s,t}(x) = |\det K_{a,s}|^{-1/2} \psi(K_{a,s}^{-1}(x-t)) \quad (14)$$

$$K_{a,s} = \begin{pmatrix} a & \sqrt{as} \\ 0 & \sqrt{a} \end{pmatrix} = BS = \begin{pmatrix} a & 0 \\ 0 & \sqrt{a} \end{pmatrix} \begin{pmatrix} 1 & s \\ 0 & 1 \end{pmatrix} \quad (15)$$

where S is an anisotropic scaling matrix with a scaling parameter $a > 0$, and B is a shear matrix with a factor $s \in R$. B and S are both invertible matrices, with $\det S = 1$.

The shearlet mother function ψ is a composite wavelet which fulfills admissibility conditions [14, 21]. The Meyer wavelet with a good localization ability in

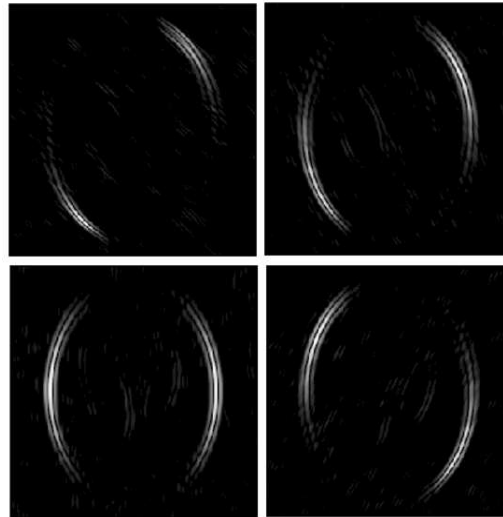


Fig. 1: Original phantom and its shearlet transformation coefficients (first scale with four different directions).

both time and frequency spaces is exploited as a mother wavelet for $\psi(\omega_x)$ in the shearlet transformation.

Beside its localization properties Meyer wavelet filters are directly described in the frequency space by $\Psi(\omega) = \Psi_1(\omega_x) \Psi_2(\omega_y/\omega_x)$ with $\omega = [\omega_x, \omega_y]$, $\Psi_1(\omega_x)$ being Fourier transform of the wavelet function and $\Psi_2(\omega_y)$ is a compactly supported bump function $\Psi_2(\omega_y) = 0 \leftrightarrow \omega_y \notin [-1, 1]$ [22, 23].

Fig. 1 shows the shearlet transformation subbands coefficients with four different directions in the first scale, applied to SheppLogan phantom image (in the remainder simply called phantom) [25].

A. L. Cunha et al. in [24], have achieved a very good performance of image denoising by thresholding in the contourlet coefficients. We adopt the thresholding method in [24], for the shearlet shrinkage in shearlet-based denoising step. The threshold is calculated as in equation (16)

$$T_{i,j} = \frac{\sigma_{i,j}^2}{\sigma_{i,j,n}^2} \quad (16)$$

where $\sigma_{i,j,n}^2$ represents the n -th coefficient variance at the i -th shearing direction subband in the j -th scale,

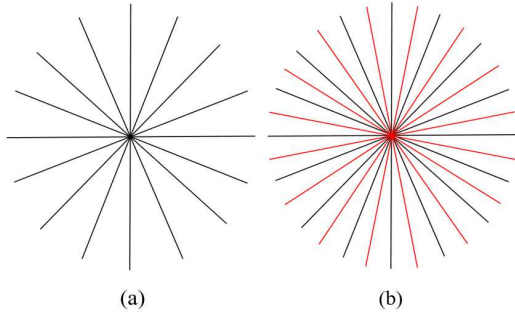


Fig. 2: (a) Original views; (b) Angular interpolation of a) for updating the geometry matrix in reprojection phase.

and $\sigma_{i,j}^2$ is the variance of noise in i -th shearing direction at scale j . $\sigma_{i,j}^2$ is estimated as follows: First, the variances for a few normalized noise images are being calculated and then we average all the estimates to get an estimate for $\sigma_{i,j}^2$. The variances of the signal in each subband are calculated by using the maximum likelihood estimator applied on all the coefficients in a square neighboring area. After thresholding the coefficients, we reconstruct back $(x) \in R^2$:

$$\hat{f} = \sum_{a,s,t} S\hat{H}_\phi \psi_{a,s,t} \quad (17)$$

3.3 Reprojection

In the re-projection step, since we are dealing with the sparse-view angles, we reproject \hat{f} back to the projection space using the updated geometry matrix A . Since we all the geometry space parameters is known, in each iteration we are modifying the geometry matrix and double the number of angels we had in the first sparse-view problem. If we define the sparse-view problem with $0 : d : 360$ angles where d is a step size, then we reproject \hat{f} back into the projection space using $0 : d/2 : 360$ angles with A_{new} (Fig. 2).

$$A_{new}\hat{f} = \hat{b} \quad (18)$$

A pseudo-code of the proposed AIRR method is depicted here.

4 Numerical Results

For comparison of the proposed method and the reference methods we use the distance between the reconstructed images and the original phantom image as it was defined

```

Initial ;
While  $\|W^{1/2}(b - Af^k)\|_2 \leq \tau\delta$ 
 $f^{k+1} = f^k + \lambda_k C^{-1} V A^T W (b - Af^k)$ ;
end
 $\hat{f} = f^{k+1}$  ;
 $SH_\phi(a, s, t) = \langle \hat{f}, \psi_{a,s,t} \rangle$  ;
 $S\hat{H}_\phi = \text{Shrinkage}(SH_\phi(a, s, t), T_\alpha)$  ;
 $\hat{f} = \sum_{a,s,t} S\hat{H}_\phi \psi_{a,s,t}$  ;
 $A_{new}\hat{f} = \hat{b}$  ;
 $f = \hat{f}$  ;
goto Initial.

```

Algorithm 1: AIRR Algorithm

in [8]. The distance is calculated according to equation (19).

$$Distance = \left(\frac{\sum_{x=1}^l \sum_{y=1}^l (f_{final}(x,y) - X(x,y))^2}{\sum_{x=1}^l \sum_{y=1}^l (X(x,y))^2} \right)^{1/2} \quad (19)$$

where X is the original $l \times l$ phantom and f_{final} is the reconstructed image. *Distance* metric is the ratio of all squared differences between the reconstructed and the original phantom image to the sum of the squared pixel values in the phantom image. We validate our proposed AIRR method for the fan-beam sparse-view reconstruction in two different models, i.e., noise-free and noisy projections. l in our experiments is 256 and we use three scales and four directions in the shearlet-based denoising step. For noise-free and noisy cases, we use the models defined in equation (8) and equation (9). Noise n in equation (9) is defined as an AWG noise with $\sigma = 10$. We use 20 fan-beam projections as inputs. The noise is added to the fan-beam projections. This system settings has been selected same to those used for experiments in [8].

Fig. 3 shows the comparison between the performance of the proposed AIRR method, and the IRR and IRR-TV methods. Compared to the IRR method, the IRR-TV has shown a better performance due to the smoothing properties of the TV term that delays the divergence. The proposed AIRR method shows a slightly better performance and since the geometry matrix is updated in the reprojection step, the result does not diverge as fast as for other two methods. Fig. 4 shows the performance comparison of the methods in the noisy projection model. The IRR-TV shows the better quality in the first three iterations, but it is not stable and starts diverging after few iterations. The AIRR method has outperformed the IRR-TV in the presence of noise as well.

Fig. 5 includes the phantom sparse-view reconstruction results for the noise-free case. The AIRR reconstruction in Fig. 5 (a) has a better contrast compared to IRR-TV. There are few visible artifacts in the presence of noise as observed in Fig. 6. In order to quantify the quality of the structural representation and measure the

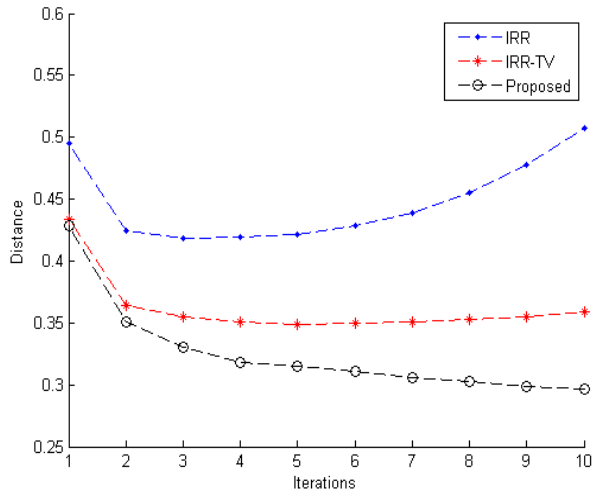


Fig. 3: Performance comparison of the IRR, IRR-TV, and the proposed AIRR in terms of the distance metric in different iterations for the noise-free case.

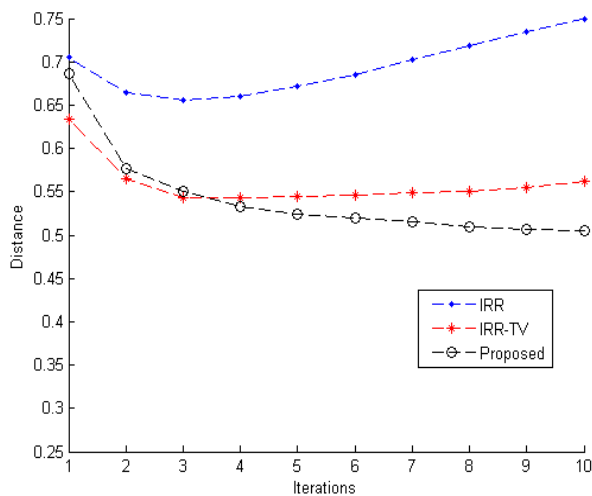


Fig. 4: Performance comparison of the IRR, IRR-TV, and AIRR in terms of the distance metric for different iterations for noisy projections case (AWG with $\sigma = 10$).

similarity between the reconstruction results and original phantom image, we calculate the structural similarity (SSIM) index [26] as a standard metric. The overall structural similarity index can be measured as follows:

$$SSIM(x, y) = \frac{(2\mu_x\mu_y + v_1)(2\sigma_{xy} + v_2)}{(\mu_x^2 + \mu_y^2 + v_1)(\sigma_x^2 + \sigma_y^2 + v_2)} \quad (20)$$

Table 1: Structural similarity indices for all the methods in noisy and noise-free cases.

Method	Noise-Free Projections	Noisy Projections
Proposed (AIRR)	0.6769	0.6169
IRR-TV	0.6692	0.5670
IRR	0.6004	0.5275

Where v_1 and v_2 are constants that stabilize the division with weak denominator and μ_x and μ_y are the local means and σ_x and σ_y are the local standard deviations. Table 1 represents the structural similarity indices. The SSIM indices for the AIRR method are best in both noisy and noise-free cases. Since we are using Shearlet-based denoising in our framework, the computational complexity of our method is at a cost of $O(n^2 \log(n))$ for a $n \times n$ image. Finally, the running time consumed by either AIRR or IRR-TV or IRR is proportional to the iteration numbers.

Future work could include the new adaptive techniques for updating the geometry matrix in reprojection phase to increase the image resolution and contrast in each loop and also could include the different regularization techniques for better reconstruction in complex scenarios including medical applications.

5 Conclusion

The paper has introduced an efficient method for solving the sparse-view CT reconstruction problem. The practical utilization of the method comes from its ability to satisfy the application requirements such as a low scan time and radiation doses. The proposed algebraic iterative reconstruction-reprojection algorithm with shearlet regularization attains a better estimation in the projection space, and as a result contributes greatly to the quality of reconstruction in terms of the distance metric, calculated based on the distance to the original image, and based on the structural content, the performance of proposed method is higher than that for the IRR-TV, which was introduced to improve the quality of the traditional IRR method.

Acknowledgement

This work was supported by NASA EPSCoR under cooperative agreement No. NNX10AR89A.

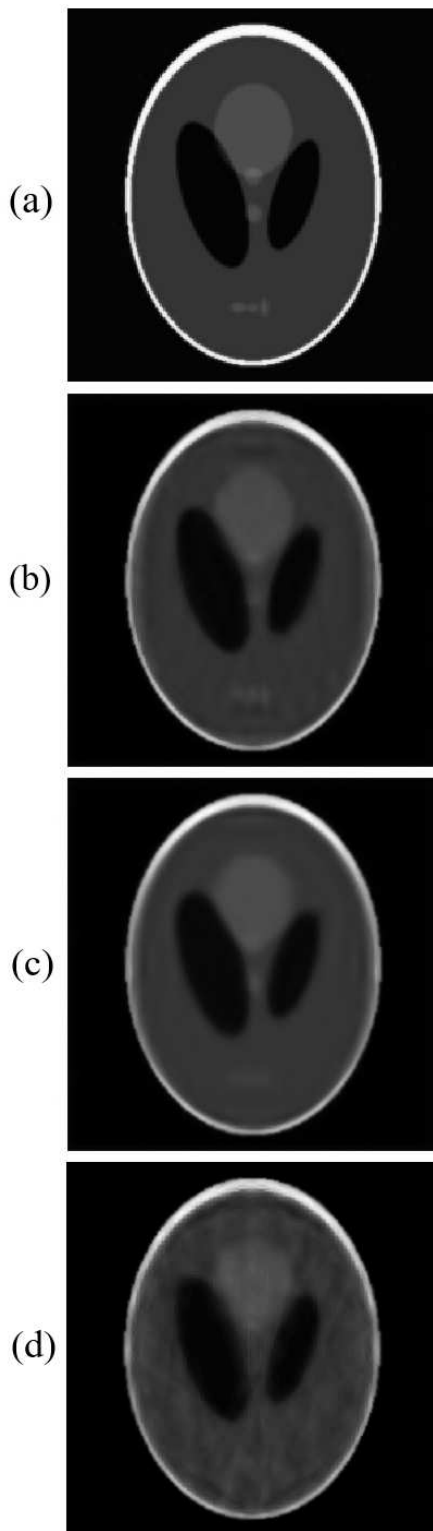


Fig. 5: (a) Original phantom image. (b) The AIRR reconstruction, (c) IRR-TV reconstruction, and (d) IRR reconstruction; from the noise-free sparse-view projections.

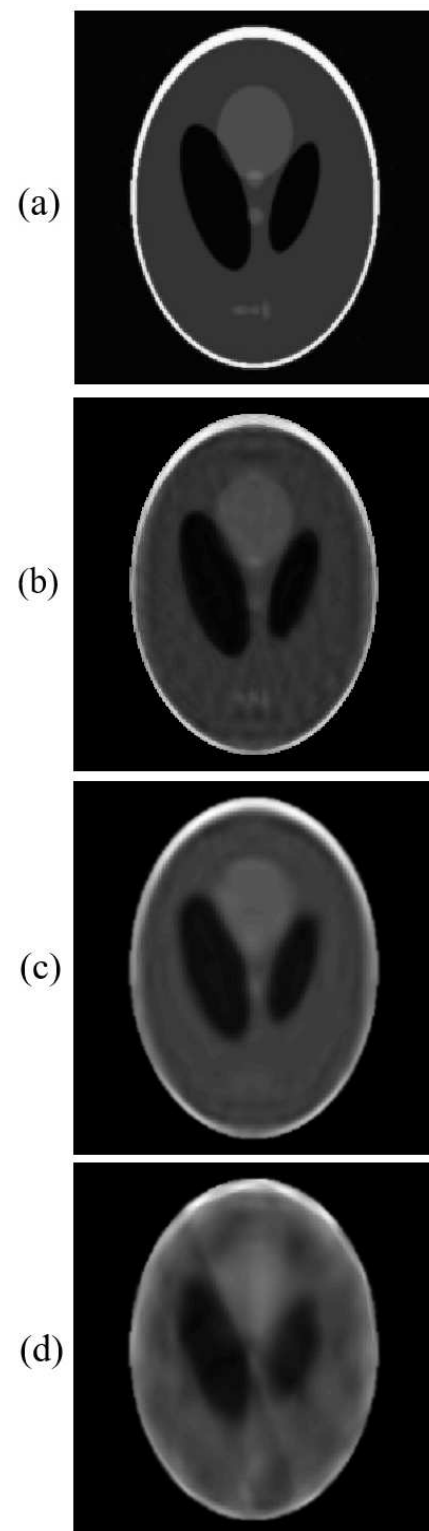


Fig. 6: (a) Original phantom image. (b) The AIRR reconstruction, (c) IRR-TV reconstruction, and (d) IRR reconstruction; from the noisy sparse-view noisy projections.

References

- [1] J. Clayton, D. Shedlock, S. Vanderet, G. Zentai, J. Star-Lack, R. LaFave, and G. Virshup, Prototype 1.75 MV X-band linear accelerator testing for medical CT and industrial nondestructive testing applications, Proc. SPIE **9438**, Health Monitoring of Structural and Biological Systems, (2015).
- [2] H. Zhang, Y. Sun, and L. Wei, Explosives detection method based on improved algebraic reconstruction technique. Intelligent Control and Automation, WCICA 2008. 7th World Congress on, 17641767 (2008).
- [3] L. W. Goldman, Principles of CT and CT technology, J. Nuclear Med. Technol. **35**, 115128 (2007).
- [4] E. Riveros, The digital radiographic and computed tomography imaging of two types of explosive devices. Applied Radiation and Isotopes. **57**, No. 6, 861865 (2002).
- [5] J. H. Kim, K. Y. Kwak, S. B. Park, and Z. H. Cho. Projection Space Iteration Reconstruction-Reprojection. IEEE Transactions on Medical Imaging, **4**, No. 3, (1985).
- [6] M. Nassi, R. B. William, B. P. Medoff, and A. Macovski. Iterative Reconstruction-Reprojection: An Algorithm for Limited Data Cardiac-Computed Tomography. IEEE Transactions on Biomedical Engineering. **29**, No. 5, (1982).
- [7] E. Candes, J. Romberg, and T. Tao, Robust uncertainty principles: Exact signal reconstruction from highly incomplete frequency information. IEEE Transaction on Information Theory. **52**, No. 2, 489509 (2006).
- [8] Xinhui Duan, Li Zhang, Yuxiang Xing, Zhiqiang Chen, and Jianping Cheng. Few-View Projection Reconstruction with an Iterative Reconstruction-Reprojection Algorithm and TV Constraint. IEEE Transaction on Nuclear Science. **60**, No. 5, 3305-3317 (2009).
- [9] G.R. Easley, D. Labate, F. Colonna. Shearlet-based total variation diffusion for denoising. IEEE Trans Image Process. **18**, No. 2, 260-268 (2009).
- [10] Y. Li, R. Chen, S. Liang. A New Image Denoising Method Based on Shearlet Shrinkage and Improved Total Variation, Intelligent Science and Intelligent Data Engineering, Vol.7202, Lecture Notes in Computer Science, pp. 382-388 (2012).
- [11] R. Gerchberg. Super-resolution through error energy reduction. Journal of Modern Optics. **21**, No. 9, 709720 (1974).
- [12] A. Papoulis. A new algorithm in spectral analysis and band-limited extrapolation. IEEE Transaction on Circuits and Systems. **22**, No. 9, 735742 (1975).
- [13] Y. Censor and T. Elfving. Block-iterative algorithms with diagonally scaled oblique projections for the linear feasibility problem, SIAM. **24**, 40-58 (2002).
- [14] B. Vandeghinste, B. Goossens, R. V. Holen, C. Vanhove, A. Pizurica, S. Vandenberghe, and S. Staelens. Iterative CT Reconstruction Using shearlet-Based Regularization. IEEE Transaction on Nuclear Science. **60**, No. 5, 3305-3317 (2013).
- [15] M. Jiang and G. Wang. Convergence of the Simultaneous Algebraic Reconstruction Technique (SART). IEEE Transaction on Image Process, **12**, No. 8, (2003).
- [16] K. D. Sauer and C. A. Bouman. A local update strategy for iterative reconstruction from projections. IEEE Transaction on Signal Processing, **41**, No. 2, 534548 (1993).
- [17] K. Guo and D. Labate. Optimally sparse multidimensional representation using shearlets. SIAM J. Math. Anal., **39**, No. 1, 298318, (2007).
- [18] G. R. Easley, D. Labate, and W.-Q. Lim. Sparse directional image representations using the discrete shearlet transform. Appl. Comput. Harmon. Anal. **25**, No. 1, 2546 (2008).
- [19] G. Kutyniok and D. Labate. Resolution of the wavefront set using continuous shearlets. Trans. Amer. Math. Soc. **361**, No. 5, 27192754 (2009).
- [20] S. Yi, D. Labate, G. R. Easley, and H. Krim. A shearlet approach to edge analysis and detection. IEEE Trans. Image Processing. **18**, No. 5, 929941 (2009).
- [21] K. Guo, D. Labate, and W.-Q. Lim. Edge analysis and identification using the continuous shearlet transform. Appl. Comput. Harmon. Anal., **27**, No. 1, 2446 (2009).
- [22] B. Goossens, J. Aelterman, H. Q. Luong, A. Piurica, and W. Philips. Efficient design of a low redundant discrete shearlet transform. Proc. Int. Workshop Local and Non-Local Approximation in Image Processing, 112124 (2009).
- [23] I. Daubechies, Ten Lectures on Wavelets. Philadelphia, PA, USA: SIAM, (1992).
- [24] A. L. Cunha, J. Zhou, and M. N. Do. The non-sampled contourlet transform: Theory, design, and applications, IEEE Transactions on Image Processing. **15**, 30893101 (2006).
- [25] L.A. Shepp and B. F. Logan. Reconstructing interior head tissue from X-ray transmissions. IEEE Trans. Nucl. Sci., **NS-21**, No. 1, 228236 (1974).
- [26] Z. Wang, A. C. Bovik, H. R. Sheikh, and E. P. Simoncelli, Image Quality Assessment: From Error Visibility to Structural Similarity. IEEE Transactions on Image Processing. **13**, No. 4, 600612 (2004).



Ali Pour Yazdanpanah

received his B.S. and M.S. degrees in Electrical and Computer Engineering from University of Science and Research, Tehran, Iran (2007, 2010). He is working toward his Ph.D. degree in Electrical and Computer Engineering

at University of Nevada since 2012. His interests include image processing, computer vision, inverse problem, mathematical optimization, embedded signal processing.



Emma E. Regentova

received her PhD in Computer Engineering from State Engineering University of Armenia. She is currently a professor in the Electrical and Computer Engineering Department, University of Nevada, Las Vegas (UNLV). She is working in the field of classical and applied image

processing.



George Bebis received his BS degree in Mathematics from the University of Crete in 1987, the MS degree in Computer Science from the University of Crete in 1991, and the PhD degree in Electrical and Computer Engineering from the University of Central Florida in 1996. He is currently a Professor in the Department of Computer Science and Engineering at the University of Nevada, Reno (UNR), director of UNRs Computer Vision Laboratory (CVL), and Visiting Professor at King Saud University. Prior to joining UNR, he was a Visiting Assistant Professor in the Department of Mathematics and Computer Science at the University of Missouri-St. Louis (UMSL).